



Contents lists available at ScienceDirect

# Journal of Computational and Applied Mathematics

journal homepage: [www.elsevier.com/locate/cam](http://www.elsevier.com/locate/cam)

## Automatic roughness characterization of simulated ice shapes

Mariachiara Gallia\*, Tommaso Bellosta, Alberto Guardone

Department of Aerospace Science and Technology, Via La Masa, 34, Milan, 20156, Lombardia, Italy



### ARTICLE INFO

#### Article history:

Received 30 October 2022

Received in revised form 19 January 2023

#### Keywords:

In-flight icing

Ice accretion

Roughness

Self-organizing maps

### ABSTRACT

During in-flight ice accretion, roughness plays an important role since it heavily influences the convective heat transfer and skin friction coefficients. This paper aims to assess the ability of existing ice accretion simulation tools to compute the growing ice's roughness. To this purpose, a technique based on Self Organizing Maps is applied to numerical simulations of in-flight ice accretion to characterize the roughness. The numerical ice predictions are performed using a standard approach comprising RANS computations, Lagrangian particle tracking, the solution of the unsteady Stefan problem, and a morphogenetic model. Numerical simulations are performed on selected benchmark cases from the 1st AIAA Ice Prediction Workshop. Validation of roughness computation is performed on synthetic test cases, while ice roughness is compared directly to that extracted from ice scans. The results of simulated ice shapes compare reasonably well with experimental data. Computations can replicate the trend of the experimental mean ice shape and roughness distribution for both rime and glaze cases.

© 2023 Elsevier B.V. All rights reserved.

## 1. Introduction

In-flight ice accretion is an important issue in aircraft design, and aviation safety [1]. It may possibly lead to a degradation of the aerodynamic properties of wings, and disturb the output of sensors and engine performances. The growing concerns about the in-flight icing issue, and the increased attention of regulators and manufacturers in addressing safety concerns, led to a blossoming of the related research activity. The early work of Stefan [2], and Messinger [3] built the foundation for all subsequent research efforts, first of which the work of Myers [4]. Currently, literature reports a wide variety of numerical prediction codes, coming from either academia or industry and government-founded agencies [5–9]. Numerical tools provide a mean to predict ice formation at critical locations over the aircraft fuselage and wings. Codes are exploited to complement the experimental activity required to design new aircraft. Moreover, comparing predictions against observations allows for model testing and tuning.

Airworthiness standards now require modern large civil aircraft to sustain operations in ice accretion conditions. Often, numerical simulation is the only viable means to design for such requirements, it being inexpensive and safe compared to in-flight or wind tunnel testing. Therefore, the accuracy and reliability of the numerical tools are extremely important. Roughness is expected to play an important role in ice accretion. First, it heavily influences the convective heat transfer coefficient by exposing an increased surface to the flow. Enhanced convection leads to higher ice growth rates. Second, roughness that forms at the early stages of accretion can trip the boundary layer to a premature transition, which modifies not only the heat transfer, but also the skin friction coefficient is perturbed [10]; this is the main driving force of the liquid film, and its motion is crucial in glaze ice conditions. Therefore, an accurate characterization of icing roughness would

\* Corresponding author.

E-mail address: [mariachiara.gallia@polimi.it](mailto:mariachiara.gallia@polimi.it) (M. Gallia).

## Nomenclature

### Greek letters

$\epsilon$  Relative Error

### Parameters

$\bar{y}$  Average Height [m]  
 $\mathbf{x}$  Point of the Data Cloud [m]  
 $dN$  Normal Distance of point of the Data Cloud from Code Book Vector [m]  
 $R_a$  Mean Arithmetic Roughness [m]  
 $s$  Curvilinear Abscissa [m]  
 $S_a$  Arithmetic Mean Height [m]  
 $y(x)$  Height [m]

lead to a more precise estimation of the convective heat transfer and the skin friction if this information is propagated to the aerodynamic solver. Recent results available in the literature show that improved roughness modeling leads to more accurate predictions [11]. Current numerical codes either consider a constant roughness [5] or implement some experimental correlation [12] or analytical model [13]. As such, current roughness modeling cannot cover all possible ice accretion regimes and the effect of different geometries. This work aims to assess the ability of existing ice accretion simulation tools to compute the roughness of the simulated ice shapes. The requirement is that numerical results must attain an accuracy comparable with experimental results. This would provide a new tool for the characterization and comparison of experimental and simulated ice shapes. Another use of the present research effort is providing a more extended database of roughness measurements to cover more geometries and icing conditions, leading to a better understanding of roughness evolution during ice accretion.

The paper is structured as follows. In Section 2 the computational model is briefly described. In Section 3, the Self Organizing Maps approach to compute the ice roughness is introduced. Section 4 presents the results obtained with the proposed framework. Finally, in Section 5 conclusions are drawn.

## 2. Ice accretion simulation

The numerical simulation of in-flight ice accretion often is built on the assumption that the phenomenon, although time dependent, can be approximated as quasi-steady. Although fully coupled, unsteady icing simulations are possible (see, e.g., [14]), the quasi-steady approximation is justified by the much longer time scale of ice accretion to that of aerodynamic problem. In addition, the low concentration of water droplets in the air makes the flow solution independent from the particle phase and can thus be obtained in an uncoupled manner [15,16]. Using the quasi-steady approximation, the total ice accretion is subdivided into smaller layers to reach the final icing time. The multi-stepping approach aims to account for the feedback of the growing ice on the aerodynamic and droplet fields. The total number of steps to employ is somewhat case-dependent, and no unique solution is reported in the literature. Usually, ten steps are used for large 3D simulations, and more can be used in 2D, see e.g. [17,18]. The goal is to accrete small layers so that changes in the aerodynamic and droplet fields are negligible. Also, the type of accretion influences the number of steps to be used. Icing in the rime regime usually requires fewer layers than in the glaze regime. If the total exposure time is accreted in a single layer, the simulation uses a single-step (or single-shot) approach.

In-flight icing simulation frameworks are usually composed of four tools: an aerodynamics solver, a solver for the particle phase, a thermodynamic module to compute the accretion rate, and a geometry tool to output a valid volume mesh that complies with the new iced geometry. The solution procedure follows the pipeline reported in Fig. 1. Using the quasi-steady approximation, each step is taken sequentially. First, the airflow is computed around the current geometry. This work uses a Finite Volume discretization to obtain a solution to the Reynolds-averaged Navier Stokes equations. Then, the water collected by the aircraft's surfaces is computed by simulating the evolution of the droplets through the computational domain. Mass and energy balance is solved on the surface grid, and an ice layer is generated. If the total time of the icing event is not yet reached, a new computational mesh is obtained for the iced configuration, and the whole process is repeated. In the following the main components of the simulation framework are briefly discussed.

### 2.1. The aerodynamic model

The aerodynamic solution is obtained as the solution of a viscous compressible turbulent flow modeled by the Reynolds Averaged Navier Stokes (RANS) equations. The effects of turbulence on the mean flow are modeled using the Boussinesq hypothesis which amounts to an increase in the viscosity. The total viscosity is obtained as the sum of the laminar viscosity

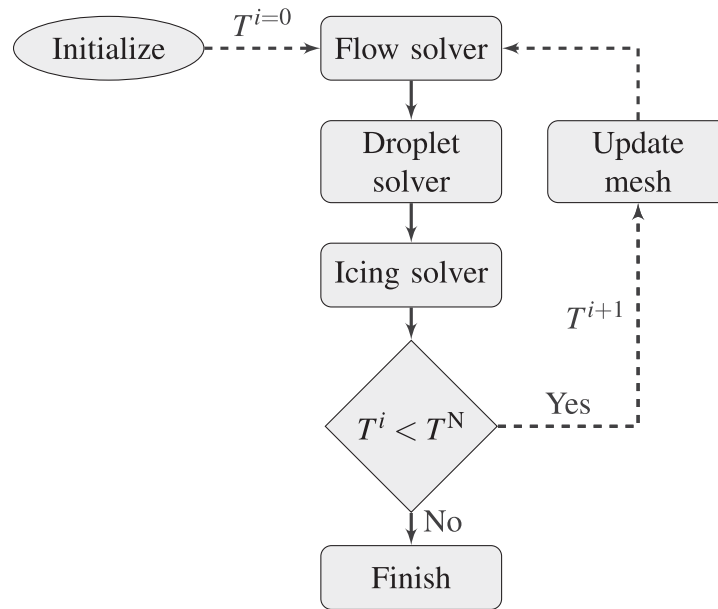


Fig. 1. Block diagram showing the common workflow in an icing simulation.

and the turbulent one. Laminar viscosity is computed via the model of Sutherland [19]. The turbulent viscosity is obtained as the solution of the one-equation model of Spalart–Allmaras [20]. The open-source SU2 code is used to compute the solution of the RANS system [21]. The compressible RANS equations are discretized using a vertex-based finite volume method. The solver operates on a median-dual grid through an edge-based data structure. The convective fluxes are discretized using a limited second-order MUSCL reconstruction [22] with the slope limiter of Venkatakrishnan [23]. The Riemann problem is solved at each edge to compute the fluxes via the approximate solver of Roe [24]. Viscous fluxes are discretized using the corrected average of gradients method, while source terms are approximated at each node using a piece-wise constant reconstruction within each control volume. Gradients are obtained via a weighted least-squares method [25]. A time-marching approach drives the system to a steady state using an implicit Euler scheme. The resulting sparse linear system is solved via a quasi-newton iteration using the GMRES solver [26]. Local time stepping and automatic CFL adaptation coupled with under-relaxation is employed to accelerate convergence [27].

## 2.2. The droplet model

An in-house particle tracking code based on a Lagrangian framework was developed at Politecnico di Milano and is used for the simulation of clouds containing supercooled water droplets [28]. The aim of the droplet solver is that of computing the collection efficiency  $\beta$  over the aircraft, which is used to compute the water mass that is collected at a given location on the surface. The Lagrangian framework allows to track each particle motion in the flow field by integrating its equation of motion. Therefore, the modeling of super-cooled water droplets effects, such as splashing effects, aerodynamic breakup, deformation is straightforward and it can deal with secondary particles. The cloud impinging the aircraft surfaces, is represented as a single front initially placed at an arbitrary distance ahead of the aircraft. This distance is set so that droplets are traced starting from an unperturbed region of the domain and so that the computational burden related to the trajectory time integration, proportional to the integration length, is bearable. In three-dimensional problems, this front consists of a two-dimensional layer of droplets uniformly distributed. In a two-dimensional setting the layer degenerates into a straight line. As the final result depends on the particle resolution, a strategy was developed to automatically refine the seeding region by adding new particles where needed. The seeding front, initially uniform, is discretized as a structured mesh of linear (in 2D) or quadrilateral (in 3D) elements. Elements are incrementally split at each iteration which consists of evolving the current cloud front and computing  $\beta$  on the surface. The simulation stops when the difference in  $L2$  norm between two consecutive collection efficiency calculations is below a user supplied threshold. In practical applications, clouds are poly-dispersed. A standard approach deals with this problem by tracking a uniform cloud of droplets with diameter equal to the Median Volume Diameter (MVD). That is the particle size that divides the total mass of the cloud in two. Half the mass is coming from droplets of diameter smaller than the cloud MVD, half from particles larger than the MVD. A more refined discretization of the particle size distribution can be taken into account by subdividing the droplets size probability distribution function in a given number of bins. For each bin, a simulation can be performed and the final collection efficiency can be obtained as a weighted sum of the bins'  $\beta$ .

### 2.3. The freezing model

The morphogenetic approach [29] is used to generate the ice shapes. First introduced to model ice accretion on power lines' cables [30], and then extended to in-flight icing [9], the morphogenetic approach models the ice accretion phenomenon as a stochastic process, tracking single fluid parcels in a Lagrangian frame of reference. The stochastic algorithm works on a 3D uniform cartesian grid that envelops the target surface or part of it. Voxels of the grid represent the fluid elements, which can be thought of as a group of droplets undergoing an average time history described by the motion of the fluid element. The model mimics the physical process leading to ice accretion by simulating particles impinge the surface and subsequently freezing. Fluid elements are sequentially shot toward the surface from a straight line aligned to the local droplets velocity, in a way such to comply with the surface water distribution obtained with the Lagrangian solver described in Section 2.2. Fluid particles can either impinge on the clean geometry or the already accreted ice. At the impingement location, fluid elements can freeze or begin a (biased) random walk on the iced surface in the direction of the local skin-friction coefficient. The parameter governing the freezing, or lack thereof, is the freezing probability known on the wing surface. At each point in the random walk, a pseudo-random number is generated and compared with the local freezing probability. If the fluid element can freeze, it does so at a close location where it maximizes the number of occupied neighbors.

The freezing probability is defined as the freezing fraction on the aircraft surface, i.e. the amount of freezing water mass divided by the total mass of water, which can either come from the impinging droplets or from water flowing from the neighboring locations. In the original work of Szilder [29], the freezing probability is computed using the model of Messinger [3], which amounts to solving a mass and energy balance on the wing surface. In the present work, we employ an extension of the model of Myers [4], which considers also the temperature profile in the ice and water layers. In particular we employ a local exact solution of the unsteady Stefan problem to obtain the freezing rate in the glaze case [31]. To do so, this work makes use of PoliMIce, the ice accretion code developed at Politecnico di Milano [5]. The freezing probability is computed on the aircraft surface by PoliMIce beforehand, and it is given as an input to the morphogenetic model together with the surface distributions of the collected mass of supercooled water, the impinging droplets velocity, and the skin friction.

With the morphogenetic model, the ice volume is constructed by sequentially freezing groups of particles. This creates ice accumulations that can contain voids, in an analogy with air bubbles being trapped inside forming ice, and present complex morphologies. Also, the resulting ice surface is uneven and rough.

In this work, we employ single-step icing simulations. Such an approach is applicable to short-time icing events, where the growth of ice on the geometry only slightly changes the aerodynamics and particles fields. Even so, we simulate longer accretion events with the aim of comparing the ice shape predicted with the morphogenetic approach, against experimental data. The ballistic nature of the stochastic model is able to account for shadowing effects, and may produce better results than a standard single-step model.

### 3. Self organizing maps for roughness characterization

Self-organizing maps (SOM) is an unsupervised machine learning technique commonly used to determine non-linear manifolds starting from a data point cloud [32,33]. The data is fed to the algorithm that takes the position of each point of the point cloud,  $\mathbf{x}$ . Then, the codebook vectors (CBV) are initialized. These are moved toward the centroid of a cluster of points that will have the CBV as the Best Matching Unit (BMU). This is done for all CBVs through a batch training procedure. Once the training is completed, the result is a map of CBV that identifies the mean shape of the point cloud. Finally, once the mean shape is known, statistical quantities related to the data point cloud can be computed. In this case, the mean arithmetic roughness  $R_a$ , defined as the average distance of each input data point from the mean shape. For each point of the clump, the normal distance  $dN$  from its BMU is computed, and for each CBV  $R_a$  is computed as:

$$R_a = \frac{1}{n} \sum_{i=1}^n |dN_i| \quad (1)$$

where  $n$  is the number of points belonging to that data clump. In the context of roughness characterization for in-flight icing, this approach has already been used to evaluate the mean shape and roughness from an experimental ice scan [33–35]. Other techniques exist that, for example, unwrap the experimental data on a distance-spanwise-radial coordinate system and then compute the mean ice shape and the roughness. The main advantage of SOM compared to these other classical techniques is that it can be applied also to complex geometries like glaze ice shapes where the projection method would fail. Indeed, a one-to-one correspondence between the clean wing and the ice shape is missing. To the best of our knowledge, the SOM technique has never been used to characterize the roughness of simulated ice shapes. The SOM algorithm needs as input a data point cloud that represents the external surface of the ice shape. First, a morphogenetic ice accretion simulation is performed as described in Section 2.3. Then, using a front advancing technique the external surface is extrapolated and given as input to the SOM numerical code which performs the computation and returns the mean shape grid identified by the CBV and the corresponding mean arithmetic roughness.

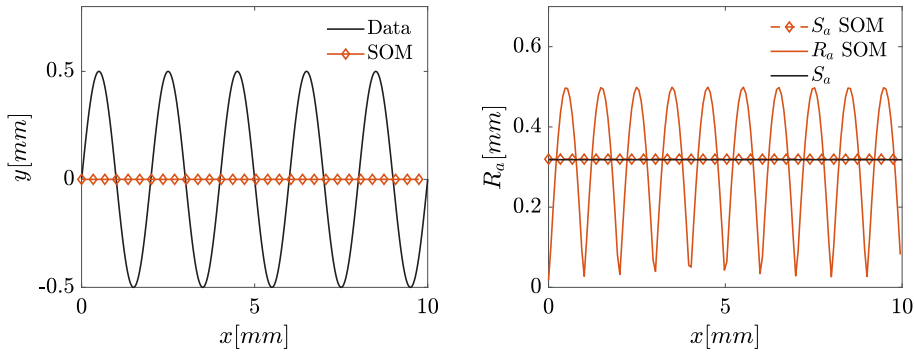


**Fig. 2.** Flat Plate with sinusoidal roughness. Left, data point cloud and mean shape obtained with SOM. Right,  $R_a$  along the flat plate and arithmetic mean height  $S_a$  computed from SOM and analytically.

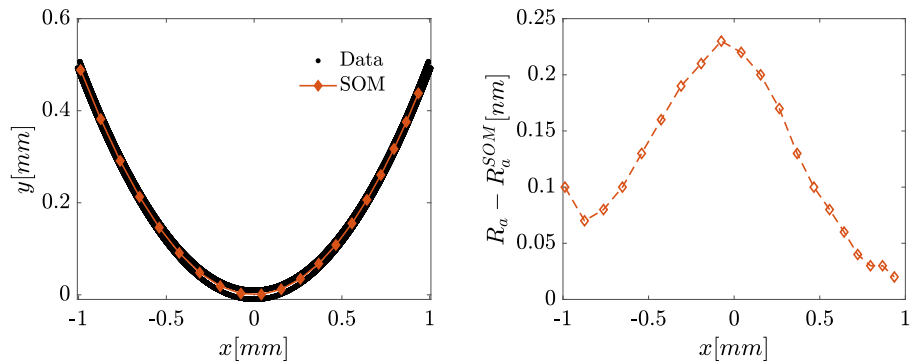


**Fig. 3.** Parabola with uniform roughness of  $R_a = 0.01$  m. Left, data point cloud and mean shape obtained with SOM. Right, difference between the imposed and computed  $R_a$  along the curvilinear abscissa, positive value refers to the parabola's right while negative to the left.

## 4. Results

### 4.1. Roughness computation validation

Before analyzing the roughness of ice scans and simulated ice shapes, a validation on simpler geometries has been carried out to assess the SOM algorithm capabilities. The code validation is performed by analyzing the mean shape predicted by the SOM and the computed mean arithmetic roughness  $R_a$  on synthetic test cases. First, a flat plate with a sinusoidal roughness  $y(x) = \frac{1}{2}\sin(\pi x)$  has been tested. The data point cloud and the mean shape are shown in Fig. 2. The right figure shows the  $R_a$  predicted using the SOM algorithm as in Eq. (1), along with the arithmetic mean height  $S_a$  that is defined as:

$$S_a = \frac{1}{L} \int_0^L |y(x) - \bar{y}| \quad (2)$$

for this test case the analytical computed value is  $S_a = 0.3183$  mm, while the computed value using SOM is  $S_a = 0.3179$  mm with a relative error of  $\epsilon = 0.13\%$ . The second test has been performed considering a parabola with an imposed uniform roughness of  $R_a = 0.01$  m; the results obtained are shown in Fig. 3. The left figure shows the data point cloud and the mean shape predicted by the SOM algorithm, while the right figure compares the imposed  $R_a$  and the one evaluated using SOM. The maximum relative error is  $\epsilon = 0.0023\%$ , and it is found close to the parabola vertex where there is the highest curvature. Following these test cases, it can be stated that the SOM approach proposed in this work can accurately predict the mean shape and roughness on simple geometries.

### 4.2. Ice accretion roughness computation

The ice roughness characterization results from the simulated shapes for two test cases are now presented. These are selected from the 1st Ice Prediction Workshop [36], in particular case 241 and 242. An 18-inch NACA23012 model profile was subject to rime and glaze ice accretion in Appendix C conditions in an experimental campaign carried out at NASA IRT facility [37]. A straight wing section of 0.4 m was used for the analysis, and a C-shape topology was chosen for the

**Table 1**  
Rime ice accretion. Nominal test conditions.

Mach	Pressure [Pa]	Temperature [K]	MVD [ $\mu\text{m}$ ]	AoA [deg]	LWC [ $\text{g}/\text{m}^3$ ]
0.325	92528	250.15	30	2	0.42

**Table 2**  
Glaze ice accretion. Nominal test conditions.

Mach	Pressure [Pa]	Temperature [K]	MVD [ $\mu\text{m}$ ]	AoA [deg]	LWC [ $\text{g}/\text{m}^3$ ]
0.31	92941	266.05	15	2	0.81

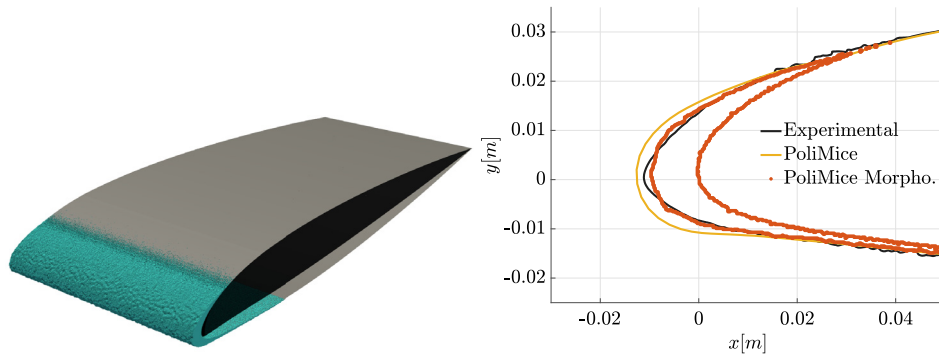


**Fig. 4.** Rime ice accretion. IPW case 241. Left, computed shape on a straight wing. Right, comparison of the predicted shape with experimental data on a cut plane.

far field. The volume was meshed with a structured grid of 1.5 million hexahedra. The Spalart–Allmaras model was used to model the effect of turbulence on the mean flow, and the collection efficiency was computed by seeding 25 million droplets in the flowfield. The fluid elements used in the morphogenetic model are voxels of size 0.2 mm.

#### 4.2.1. Rime ice

Rime ice accretion on an airfoil flying in a cloud of small droplets is now investigated. The model airfoil was exposed to the icing conditions reported in Table 1 for 5 min. Fig. 4 reports the computed ice shape. In the right picture, the ice shape obtained from PoliMice numerical simulations both with the Morphogenetic and the classical Myers model at a section in the middle of the model are compared to the experimental data. Regarding the classical ice accretion approach good agreement is found in the icing limits, while an overestimation of ice thickness is present at the leading edge. On the other hand, very good agreement in the iced volume and the position of the ice limits are shown for the morphogenetic approach. Some discrepancies can be noted at the leading edge. This could be due to the single-shot approach taken for this work. Considering the feedback of the growing ice on the aerodynamics and particles would give a closer prediction in this region. Fig. 5 reports the results obtained with the self-organizing maps approach. For this analysis a slice of 1 cm, in the middle section of the test article was taken. In the left figure, the 2D data point cloud from the experimental ice scan and the simulated ice shape is shown along with the mean shape identified by the codebook vectors. While in the right figure, the average roughness along the curvilinear abscissa is presented, positive values refer to the suction side while negative to the pressure side. As can be seen, the mean shapes are very similar in the two cases, with small discrepancies. Regarding the average roughness, the trend is similar for the experimental and simulated ice shape; there is a large discrepancy only at  $s \approx 0.04$ ; this is because there is a deviation of the simulated ice shape from the experimental scan that causes this large peak in the roughness. Since the model's base is the input data point cloud, the small discrepancy can be, once again, attributed to the single-shot approach taken for this work. Although some discrepancies can be observed in the roughness distribution, a common trend is identified. Indeed, there is a smooth region close to the stagnation point where a low roughness value is seen. Moving toward the trailing edge, the roughness is increased with two peaks, one on the pressure side and one on the suction side. Therefore, the data point distribution obtained for the simulated ice shape agrees fairly well with the experimental ice scan, both in terms of mean shape and average roughness distribution.

#### 4.2.2. Glaze ice

For the glaze ice accretion test case, the model airfoil was exposed to the icing conditions reported in Table 2 for a total of 5 min. As before, Fig. 6 shows the computed ice shape and the comparison with experimental data on a single section. Again, the computational framework with the morphogenetic approach can accurately predict the ice shape also for a glaze-type accretion. The position and height of the horns, the icing limits, and the maximum thickness are well captured for this single section. While with the classical approach, the horn position is not predicted very well but the ice

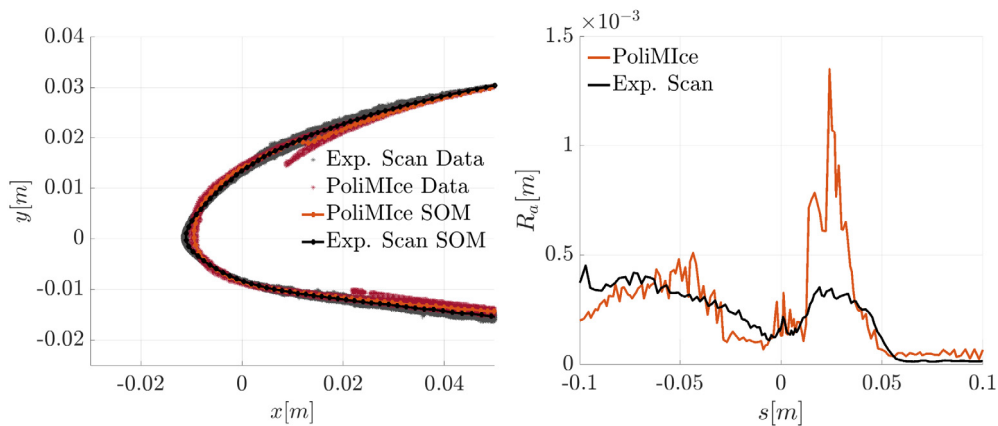


**Fig. 5.** Rime ice accretion. IPW case 241. Left, data point cloud and mean shape obtained with SOM for experimental ice scan and simulated ice shape. Right, arithmetic mean roughness computed for experimental ice scan and simulated ice shape along curvilinear abscissa, positive values refer to the suction side of the airfoil while negative to the pressure side.

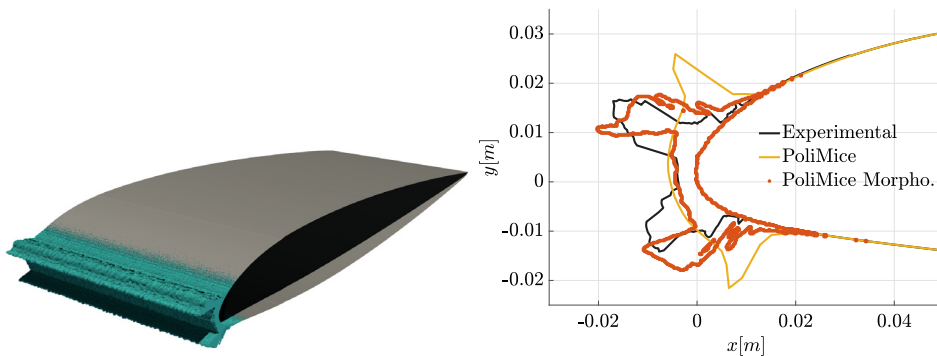


**Fig. 6.** Glaze ice accretion. IPW case 242. Left, computed shape on a straight wing. Right, comparison of the predicted shape with experimental data on a cut plane.

thickness at the stagnation point is in good agreement with experimental results. In Fig. 7 the results obtained with the self-organizing maps technique are reported. Also for this test case, a slice of 1 cm in the middle section of the test article was taken for the mean shape and roughness analysis. The left figure shows the 2D data point cloud from the ice scan and the simulated ice shape, along with the mean shapes identified by the codebook vectors. The right figure shows the average roughness along the curvilinear abscissa; positive values refer to the suction side of the airfoil while negative to the pressure side. The mean shapes are quite similar in the two cases, with small discrepancies; the numerical approach well captures the position and size of the horns. The largest discrepancy regards the plateau region in the leading edge region. Indeed, for the simulated ice shape, this is more extended compared to experimental data. This is also seen in the mean arithmetic roughness plot. The region of low roughness at the leading edge is thinner in the experimental data compared to the simulated ice shape. Although the  $R_a$  trend is similar in both cases, indeed, there is a region of low roughness at the leading edge, followed by a peak of similar magnitude in the roughness corresponding to the horn position in the ice shape. The discrepancy between simulated and experimental ice shape and roughness is higher for glaze ice conditions compared to previously presented rime ice. Once again the discrepancy is due to the different input data point cloud and could therefore be attributed to the single-shot approach used in this work. The ice shape obtained in glaze ice conditions is very different from the original airfoil, which was not the case for rime ice. Therefore, a larger influence of the modified geometry on the aerodynamic and particle trajectory is expected. Further studies should be conducted on the influence of a multi-step approach on the mean ice shape and the roughness distribution.

## 5. Conclusions

In this work, a methodology for the analysis and comparison of experimental and simulated ice shapes was presented. Self-organizing maps algorithm was used to extract the mean shape and average roughness distribution from a data point cloud. This was validated for synthetic test cases on a flat plate with a sinusoidal distribution and on a parabola with an imposed uniform roughness distribution. In both cases, the algorithm was in good agreement with the analytical

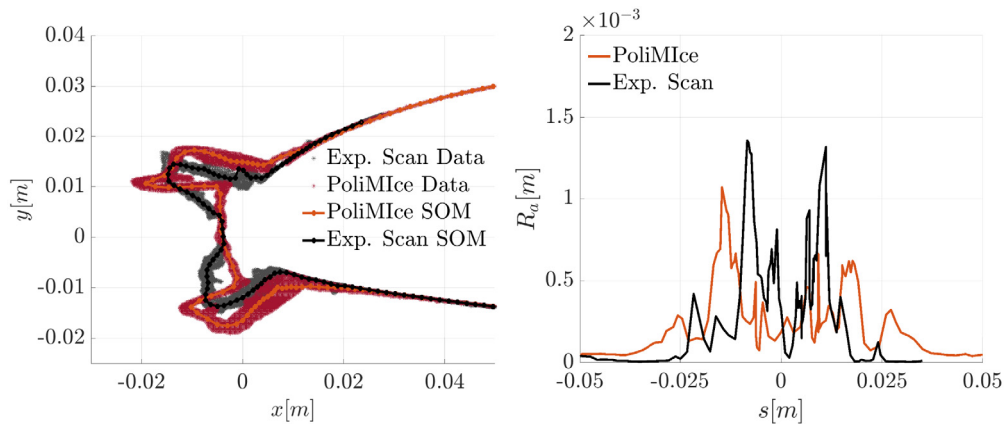


**Fig. 7.** Glaze ice accretion. IPW case 242. Left, data point cloud and mean shape obtained with SOM for experimental ice scan and simulated ice shape. Right, arithmetic mean roughness computed for experimental ice scan and simulated ice shape along curvilinear abscissa, positive values refer to the suction side of the airfoil while negative to the pressure side.

results. The methodology was then applied to two reference test cases from the 1st Ice Prediction Workshop. One for rime and one for glaze ice accretion. The simulated ice shapes were obtained with the morphogenetic approach to emulate the stochastic ice accretion process. The simulated mean ice shape and the average roughness were compared against experimental data. A very good agreement was found for rime ice accretion. On the other hand, some discrepancies were found in the glaze ice accretion test case on the mean ice shape, which then reflected on the roughness distribution. This can be attributed to the one-shot approach used for this work. Further studies will be performed on the influence of the multi-step approach on the mean ice shape and roughness. The methodology presented in this work can be a useful tool for analyzing simulated and experimental ice shapes that can be used to perform further analysis on the characterization of ice roughness.

### CRedit authorship contribution statement

**Mariachiara Gallia:** Conceptualization, Methodology, Software, Validation, Investigation, Data curation, Writing – original draft, Visualization. **Tommaso Bellosta:** Conceptualization, Methodology, Software, Validation, Investigation, Writing – review & editing. **Alberto Guardone:** Supervision, Funding acquisition, Project administration, Writing – review & editing.

### Data availability

Data will be made available on request.

### Acknowledgments

The ICE GENESIS project has received funding from the European Union's Horizon 2020 research and innovation program under grant agreement no. 824310.

### References

- [1] T. Cebeci, F. Kafyeke, Aircraft icing, *Annu. Rev. Fluid Mech.* 35 (1) (2003) 11–21, <http://dx.doi.org/10.1146/annurev.fluid.35.101101.161217>.
- [2] J. Stefan, Ueber die theorie der eisbildung im polarmeere, *Ann. Phys.* 42 (1891) 269–286, <http://dx.doi.org/10.1002/ANP.18912780206>.
- [3] B.L. Messinger, Equilibrium temperature of an unheated icing surface as a function of air speed, *J. Aeronaut. Sci.* 20 (1) (1953) 29–42, <http://dx.doi.org/10.2514/8.2520>.
- [4] T.G. Myers, Extension to the messinger model for aircraft icing, *AIAA J.* 39 (2) (2001) 211–218, <http://dx.doi.org/10.2514/2.1312>.
- [5] G. Gori, M. Zocca, M. Garabelli, A. Guardone, G. Quaranta, PoliMIce: A simulation framework for three-dimensional ice accretion, *Appl. Math. Comput.* 267 (2015) 96–107, <http://dx.doi.org/10.1016/j.amc.2015.05.081>.
- [6] T. Hedde, D. Guffond, ONERA three-dimensional icing model, *AIAA J.* 33 (6) (1995) 1038–1045, <http://dx.doi.org/10.2514/3.12795>.
- [7] G. Mingione, V. Brandi, Ice accretion prediction on multielement airfoils, *J. Aircr.* 35 (2) (1998) 240–246, <http://dx.doi.org/10.2514/6.1997-177>.
- [8] W. Wright, *User's Manual for LEWICE Version 3.2*, Contractor Report NASA/CR-2008-214255, NASA, 2008.
- [9] K. Szilder, E.P. Lozowski, Simulation of airfoil icing with a Novel Morphogenetic model, *J. Aerosp. Eng.* 18 (2) (2005) 102–110, [http://dx.doi.org/10.1061/\(ASCE\)0893-1321\(2005\)18:2\(102\)](http://dx.doi.org/10.1061/(ASCE)0893-1321(2005)18:2(102)).
- [10] F. Caccia, A. Guardone, Numerical simulation of ice accretion on wind turbine blades, *Wind Energy Sci. Discuss.* 2022 (2022) 1–27, <http://dx.doi.org/10.5194/wes-2022-43>, <https://wes.copernicus.org/preprints/wes-2022-43/>.

- [11] H. Beaugendre, F. Morency, FENSAP-ICE: Roughness effects on ice accretion prediction, in: 41st Aerospace Sciences Meeting and Exhibit, 2003, <http://dx.doi.org/10.2514/6.2003-1222>.
- [12] S.T. McClain, M.M. Vargas, J.-C. Tsao, A.P. Broeren, A model for ice accretion roughness evolution and spatial variations, in: AIAA AVIATION 2021 Forum, 2021, <http://dx.doi.org/10.2514/6.2021-2641>.
- [13] G. Fortin, A. Ilinca, J.-L. Laforte, V. Brandi, New roughness computation method and geometric accretion model for airfoil icing, *J. Aircr.* 41 (1) (2004) 119–127, <http://dx.doi.org/10.2514/1.173>.
- [14] C.N. Aliaga, M.S. Aubè, G.S. Baruzzi, W.G. Habashi, FENSAP-ICE-unsteady: Unified in-flight icing simulation methodology for aircraft, rotorcraft, and jet engines, *J. Aircr.* 48 (1) (2011) 119–126, <http://dx.doi.org/10.2514/1.C000327>.
- [15] M. Hess, P. Koepke, I. Schult, Optical properties of aerosols and clouds: The software package OPAC, *Bull. Am. Meteorol. Soc.* 79 (5) (1998) 831–844, [http://dx.doi.org/10.1175/1520-0477\(1998\)079%3C0831:OPOAAC%3E2.0.CO;2](http://dx.doi.org/10.1175/1520-0477(1998)079%3C0831:OPOAAC%3E2.0.CO;2).
- [16] S. Elghobashi, On predicting particle-laden turbulent flows, *Appl. Sci. Res.* 52 (4) (1994) 309–329, <http://dx.doi.org/10.1007/BF00936835>.
- [17] I.A. Ozcer, C. Aliaga, A. Pueyo, Y. Zhang, H. Fouladi, S. Nilamdeen, J. Selvanayagam, S. Shah, Ansys - Bombardier 1st ice prediction workshop results, in: AIAA AVIATION 2022 Forum, 2022, <http://dx.doi.org/10.2514/6.2022-3311>.
- [18] A. Donizetti, T. Bellosta, A. Rausa, B. Re, A. Guardone, Level-set mass-conservative front-tracking technique for multistep simulations of in-flight ice accretion, *J. Aircr.* (2023) 1–11, <http://dx.doi.org/10.2514/1.C037027>.
- [19] W. Sutherland, The viscosity of gases and molecular force, *Lond. Edinb. Dublin Philos. Mag. J. Sci.* 36 (223) (1893) 507–531, <http://dx.doi.org/10.1080/14786449308620508>.
- [20] P. Spalart, S. Allmaras, A one-equation turbulence model for aerodynamic flows, *AIAA* 439 (1992) <http://dx.doi.org/10.2514/6.1992-439>.
- [21] T.D. Economon, F. Palacios, S.R. Copeland, T.W. Lukaczyk, J.J. Alonso, SU2: An open-source suite for multiphysics simulation and design, *AIAA J.* 54 (3) (2016) 828–846, <http://dx.doi.org/10.2514/1.J053813>.
- [22] B. van Leer, Towards the ultimate conservative difference scheme. V. A second-order sequel to Godunov's method, *J. Comput. Phys.* 32 (1) (1979) 101–136, [http://dx.doi.org/10.1016/0021-9991\(79\)90145-1](http://dx.doi.org/10.1016/0021-9991(79)90145-1).
- [23] V. Venkatakrisnan, On the accuracy of limiters and convergence to steady state solutions, in: 31st Aerospace Sciences Meeting, 1993, <http://dx.doi.org/10.2514/6.1993-880>.
- [24] P. Roe, Approximate Riemann solvers, parameter vectors, and difference schemes, *J. Comput. Phys.* 43 (2) (1981) 357–372, [http://dx.doi.org/10.1016/0021-9991\(81\)90128-5](http://dx.doi.org/10.1016/0021-9991(81)90128-5).
- [25] D. Mavriplis, Revisiting the least-squares procedure for gradient reconstruction on unstructured meshes, in: 16th AIAA Computational Fluid Dynamics Conference, 2003, <http://dx.doi.org/10.2514/6.2003-3986>.
- [26] Y. Saad, M.H. Schultz, GMRES: A generalized minimal residual algorithm for solving nonsymmetric linear systems, *SIAM J. Sci. Stat. Comput.* 7 (3) (1986) 856–869, <http://dx.doi.org/10.1137/0907058>.
- [27] P. Gomes, T.D. Economon, R. Palacios, Sustainable high-performance optimizations in SU2, in: AIAA Scitech 2021 Forum, 2021, <http://dx.doi.org/10.2514/6.2021-0855>.
- [28] T. Bellosta, G. Parma, A. Guardone, A robust 3D particle tracking solver for in-flight ice accretion using arbitrary precision arithmetic, in: *Proceedings of the VII International Conference on Computational Methods for Coupled Problems in Science and Engineering*, 2019.
- [29] K. Szilder, E.P. Lozowski, Comparing experimental ice accretions on a swept wing with 3D morphogenetic simulations, *J. Aircr.* 55 (6) (2018) 2546–2549, <http://dx.doi.org/10.2514/1.C034879>.
- [30] K. Szilder, Simulation of ice accretion on a cylinder due to freezing rain, *J. Glaciol.* 40 (136) (1994) 586–594, <http://dx.doi.org/10.3189/S0022143000012478>.
- [31] G. Gori, G. Parma, M. Zocca, A. Guardone, Local solution to the unsteady Stefan problem for in-flight ice accretion modeling, *J. Aircr.* 55 (2017) 251–262, <http://dx.doi.org/10.2514/1.C034412>.
- [32] T. Kohonen, Self-organizing maps, ser, *Inf. Sci. Berlin*: Springer 30 (2001) <http://dx.doi.org/10.1007/978-3-642-56927-2>.
- [33] S.T. McClain, Manual point cloud registration for combined ice roughness and ice thickness measurements, in: AIAA AVIATION FORUM, 2016, <http://dx.doi.org/10.2514/6.2016-3590>.
- [34] T. Neubauer, R. Puffing, Assessment of ice shape roughness via automatic spacing of codebook vectors in a two-dimensional self-organizing map, in: AIAA AVIATION 2020 FORUM, 2020, p. 2806, <http://dx.doi.org/10.2514/6.2020-2806>.
- [35] T. Neubauer, W. Hassler, R. Puffing, Ice shape roughness assessment based on a three-dimensional self-organizing map approach, in: AIAA AVIATION 2020 FORUM, 2020, p. 2805, <http://dx.doi.org/10.2514/6.2020-2805>.
- [36] E. Laurendeau, S. Bourgault-Cote, I.A. Ozcer, R. Hann, E. Radenac, A. Pueyo, Summary from the 1st AIAA ice prediction workshop, in: AIAA AVIATION 2022 Forum, 2022, p. 3398, <http://dx.doi.org/10.2514/6.2022-3398>.
- [37] S. Lee, A.P. Broeren, R.E. Kreeger, M.G. Potapczuk, L. Utt, Implementation and validation of 3-D ice accretion measurement methodology, in: 6th AIAA Atmospheric and Space Environments Conference, 2014, <http://dx.doi.org/10.2514/6.2014-2613>.